Journal of Alloys and Compounds 709 (2017) 260–266

Contents lists available at ScienceDirect

Journal of Alloys and Compounds

journal homepage: http://www.elsevier.com/locate/jalcom

Pressure-induced phase transitions and insulator-metal transitions in VO_2 nanoparticles

Quanjun Li [a, b, *], Huafang Zhang [a], Chuanlong Lin [b], Fubo Tian [a], Jesse S. Smith [b], Changyong Park [b], Bingbing Liu [a, **], Guoyin Shen [b]

[a] State Key Laboratory of Superhard Materials, Jilin University, Changchun 130012, China
[b] High Pressure Collaborative Access Team (HPCAT), Geophysical Laboratory, Carnegie Institute of Washington, Argonne, Illinois 60439, USA

ARTICLE INFO

Article history:
Received 9 January 2017
Received in revised form
14 March 2017
Accepted 15 March 2017
Available online 16 March 2017

Keywords:
VO_2
High pressure
Phase transition
Metallization
Strongly correlated materials
Nanoparticles

ABSTRACT

We present pressure-induced phase transitions and metallization in VO_2 nanoparticles characterized by synchrotron x-ray diffraction, Raman spectroscopy, and infrared reflectivity measurements. The *M1-M1′-Mx* phase transitions were found in VO_2 nanoparticles upon compression. The results of IR reflectivity shown that pressure-induced metallization occurs in the *M1′* phase with increasing pressure and the sample becomes fully metallic at the transition of *M1′ to Mx*. The metallic *Mx* phase transforms to metastable mixed phases displaying insulating properties upon decompression. We attribute the pressure-induced metallization of the *M1′* phase to the strong electron correlations, while the metal-insulator transition (MIT) from the *Mx* to the mixed phases is found to be associated with the structural phase transitions. Both the electron-correlation-driven Mott transition and the structure-driven MIT can be achieved in VO_2 by applying pressure. Compared with bulk samples, the VO_2 nanoparticles exhibit larger bulk moduli and increased transition pressure due to their nanosize effects. High pressure provides an effective method to study the MIT in strongly correlated materials and paves the way for modifying electronic properties of VO_2.

© 2017 Elsevier B.V. All rights reserved.

1. Introduction

As a typical strongly correlated electron material, VO_2 has attracted considerable attention because of its reversible metal-insulator transition (MIT) at a moderate temperature of ~340 K, which is accompanied by a phase transition from a metallic rutile (*R*) phase at high temperatures to an insulating monoclinic (*M1*) phase at low temperatures [1–4]. Across the transition, VO_2 exhibits an abrupt change in electrical, magnetic and optical properties, making VO_2 an important material for smart optical, electrical and thermal switches [1–6]. Therefore, the underlying physics of the MIT is essential for various applications, which has been widely studied [1–10]. Various mechanisms, such as Mott transition [11–13], Peierls transition [14,15], and combinations of these two [16,17] have been proposed for explaining the temperature-induced MIT in VO_2. The exact nature of the underlying physics remains an active subject of debate, largely because of difficulties in decoupling the structural transition and electron correlation. Recently, high pressure was introduced to study VO_2 as an effective means, providing a way to correlate crystal structure with electronic properties and/or to decouple the electronic and structural phase transitions [6,18–23]. Some previous studies have shown that both structural phase transitions and the MIT can be achieved by pressure [18–22]. Pressure-induced metallization (PIM), different from the *M1-R* phase transition driven by temperature, was found in monoclinic VO_2 above 10 GPa [18]. High pressure x-ray diffraction (XRD) studies have shown that the metallic phase is isostructural with the starting *M1* phase [21]. These results do not support the Peierls distortion and emphasize the role of electron-electron correlation in the MIT. In addition, photo-induced metallization was observed in monoclinic VO_2 without changes in the lattice symmetry under high pressure, indicating that the MIT is driven by the strong electron correlations [6]. More recently, the phase transition from a monoclinic to another monoclinic structure in VO_2 at ~10 GPa was explained by a semiconductor-to-semiconductor transition using high pressure *in situ* resistivity measurements [22,23]. Bai et al. [22] also pointed out that the high

* Corresponding author. State Key Laboratory of Superhard Materials, Jilin University, Changchun 130012, China.
** Corresponding author. State Key Laboratory of Superhard Materials, Jilin University, Changchun 130012, China.
E-mail addresses: liquanjun@jlu.eu.cn (Q. Li), liubb@jlu.edu.cn (B. Liu).

http://dx.doi.org/10.1016/j.jallcom.2017.03.164
0925-8388/© 2017 Elsevier B.V. All rights reserved.

pressure monoclinic (*M1′*) phase is not metallic, and found a new high pressure metallic *X* phase above 34.3 GPa. They suggested that the structural transition dominates the pressure-induced insulator-to-metal transition in VO_2. Thus, contradictory conclusions regarding the mechanism of the MIT remain, in particular it is not clear whether structural phase transition or strong electron correlations play the dominant role in the MIT.

It is well known that domain structures greatly influence the properties of some strongly correlated materials [24,25]. In some previous studies of VO_2, it was considered an obstacle for clearly understanding the microscopic mechanism of the MIT [26–29]. In contrast to the bulk materials, the sizes of nanomaterials can be smaller than the characteristic domain size, such that nanomaterials can be utilized as a model system for exploring fundamental properties of VO_2 without influence from domain structures [24,27,28]. In addition, nanosized materials show various excellent properties and unique behaviors [25,30–32]. Therefore, several efforts have been made to study the MIT in VO_2 nanomaterials [24–29,33–36]. For instance, the relationship between the structural domain formation and the MIT in VO_2 nanobeams was investigated by Raman spectroscopy; a monoclinic and correlated metal phase was observed preceding the appearance of the rutile metallic phase [27]. VO_2 in ordered arrays exhibited size-dependent multipole optical resonance and transition temperatures, indicating the MIT temperature and the width of the hysteresis loop decreases with increasing particle size [34]. Surface stress mediated the Mott MIT in single-crystal VO_2 nanowires, for which the Mott insulating (*M2*) phase is critical in controlling the spatial extent and distribution of the insulating monoclinic and metallic rutile phases as well as the electrical characteristics of the transition [35]. However, the pressure effects on phase transition and the MIT in VO_2 nanomaterials are still poorly understood.

In this paper, we have studied pressure-induced phase transitions and insulator-metal transitions in VO_2 nanoparticles by synchrotron XRD, Raman spectroscopy, and infrared (IR) reflectivity spectra. *M1-M1′-Mx* phase transitions were observed upon compression, and the *Mx* phase transforms into mixed phases upon decompression.

2. Experimental

VO_2 nanoparticles with irregular morphology were synthesized through hydrothermal reaction combined with subsequent calcinations as described in a previous report [37]. The minimum dimension of the irregular nanoparticles is in the range of 100–200 nm. High pressure powder XRD experiments were performed at 16-IDB beamline of the High Pressure Collaborative Access Team (HPCAT) facility, at the Advanced Photon Source (APS), Argonne National Laboratory (ANL), and BL15U beamline of Shanghai Synchrotron Radiation Facility (SSRF). High pressure experiments were carried out in a diamond-anvil cell (DAC) with 300 μm diameter culets and rhenium as gasket material. Neon was used as pressure transmitting medium. Pressure was determined by the frequency shift of the ruby R1 fluorescence line and equation of state (EOS) of Au. The incident wavelength of the monochromatic beam was 0.4066 Å. Raman measurements were carried out using a Renishaw spectrometer with Ar^+ excitation laser (wavelength of 514.5 nm). The recovered sample from high pressure was characterized again by XRD after approximately one week. Le Bail whole-profile fits of the XRD patterns were performed using the GSAS software package [38].

The IR reflectivity spectra were collected by a Bruker Vertex 80v FTIR spectrometer and a microscope equipped with a liquid nitrogen cooled Mercury Cadmium Telluride (MCT) detector. The VO_2 slabs were obtained by pressing the VO_2 nanoparticles between the diamond anvils. The sample slabs were placed on top of a pre-indented KBr pellet in the sample chamber. KBr and ruby were used as pressure-transmitting medium and pressure gauge, respectively. The reflectivity of sample-diamond interface (R(ω)) was calculated by the following equation:

$$R(\omega) = \frac{I_R^S(\omega)}{I_R^{Air}(\omega)} \cdot \frac{I_R^{D\prime}(\omega)}{I_R^D(\omega)}$$

where $I_R^S(\omega)$ is the intensity reflected by the sample-diamond interface at each pressure, and $I_R^D(\omega)$ is the intensity reflected by the external face of the diamond anvil at each working pressure. $I_R^{Air}(\omega)$ and $I_R^{D\prime}(\omega)$ are the intensity reflected by air-diamond interface and by the external face of the diamond anvil, respectively.

3. Results and discussion

Fig. 1 shows the evolution of XRD patterns of VO_2 nanoparticles with increasing pressure. All the observed diffraction peaks can be indexed with the *M1* monoclinic structure below 14.9 GPa. All the diffraction peaks of the *M1* phase shifted to higher angles with increasing pressure, consistent with decreasing volume of the unit cells. Above this pressure, some diffraction peaks start to broaden or split as denoted by stars, indicating an isostructural phase transition from *M1* to *M1′* occurring above 15 GPa. The *M1′* phase is a distorted *M1* structure with the same space group ($P2_1/c$), which is consistent with the previous studies [21,22]. However, the phase transition pressure of the nanoparticle sample is higher than those (12–13 GPa) of the corresponding bulk samples [21,22]. Likely, nanosize contributed to the enhanced transition pressure because of the increased surface energy as observed in most nanomaterials [34–36]. With further increasing pressure, several new peaks appear at 32.2 GPa as marked with hash signs, which indicate a new

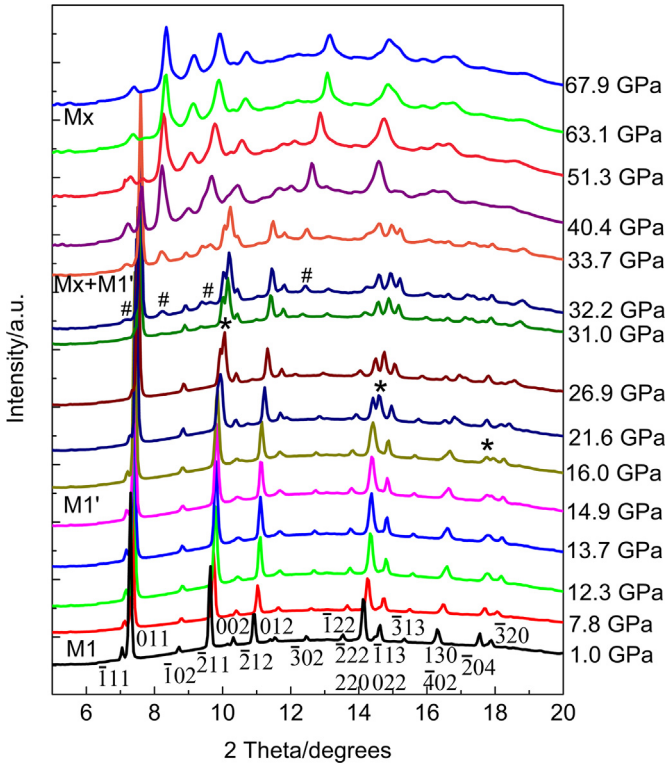


Fig. 1. High pressure XRD patterns of VO_2 nanoparticles. Stars and hash signs indicate typical diffraction peaks from the *M1′* and *Mx* phases, respectively.

phase occurring at this pressure. Above 51.3 GPa, the *M1′* phase completely transforms into the new phase, and the new phase remains stable up to the highest pressure of 67.9 GPa in this study. This result was in general agreement with the previous studies of bulk VO_2 [22].

Fig. 2 shows the unit cell parameters of the monoclinic phases (*M1* and *M1′*) as a function of pressure. The pressure dependences of the unit cell parameters were obtained by linear fits over the pressure range before and after the structural phase transition occurs at ~15 GPa. The obtained pressure coefficients of the parameters of *a*, *b*, and *c* are -8.4×10^{-3}, -6.4×10^{-3}, and -6.7×10^{-3} Å/GPa below 15 GPa, respectively. Above the transition pressure, the pressure coefficients of the parameters of *a*, *b*, and *c* are -1.0×10^{-2}, -1.1×10^{-2}, and -1.2×10^{-3} Å/GPa, respectively. It can be seen that the *b* and *c* axes exhibited obvious change in slope after ~15 GPa, while the *a* axis shown almost a continuous change with increasing pressure. Above the *M1*-*M1′* transition, the *b* axis became more compressible, while the *c* axis became less compressible. It is clear that a strong anisotropic compression took place in the *b*–*c* plane of the *M1* phase. This suggested the phase transition from *M1* to *M1′* at this pressure was associated with anisotropic compression along crystallographic directions. These results were consistent with those of the corresponding bulk material [21].

The structure of the high pressure phase above 51.3 GPa is still unclear. Various structural models (including the *X* phase in ref 22) were tested to fit the measured XRD pattern. Fig. 3 shows the structure of the high pressure phase at 67.9 GPa indexed with a monoclinic unit cell with space group $P2_1/c$ (named *Mx*). The lattice parameters were summarized in Table 1. These obtained lattice parameters of the *Mx* phase were different from those of the *X* phase in ref 22. It should be noted that the structural determination was preliminary because of the limited quality of the XRD patterns.

Upon decompression, the *Mx* phase transforms into another new structure which may be a mixture of phases. As shown in Fig. 4a, the mixed phases converted into a new phase finally after a week at ambient conditions. The XRD pattern was refined by using various structural models. A possible solution was a monoclinic structure with the same space group (named *Mx′*). The refined pattern is shown in Fig. 4b. The lattice parameters of the *Mx′* phase are listed in Table 1. It was observed that the intermediate mixed phases consisted of *Mx′* and a metastable phase which transformed into *Mx′* after a week. *Mx′* remained stable at ambient conditions.

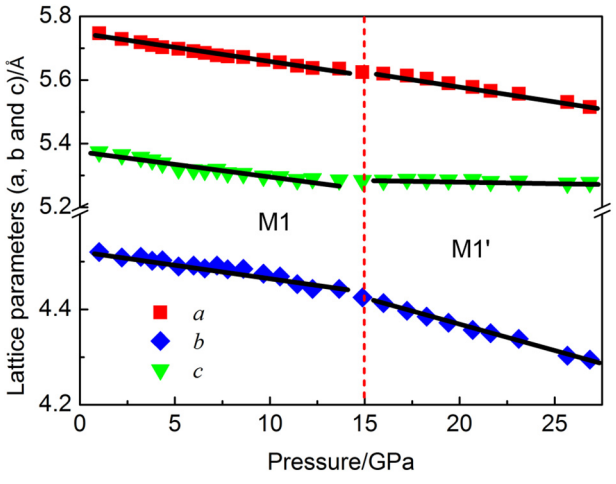


Fig. 2. Pressure dependence of *a*, *b*, and *c* unit cell parameters of the monoclinic phases (*M1* and *M1′*).

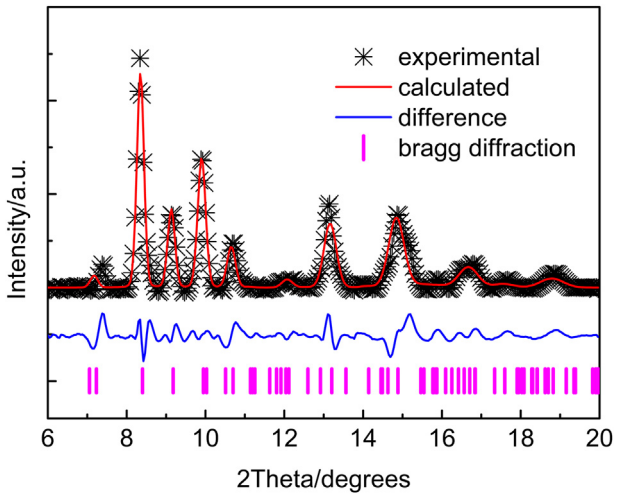


Fig. 3. The XRD pattern of the VO_2 nanoparticles at 67.9 GPa, indexed with a monoclinic unit cell with detail parameters listed in Table 1.

This is a new polymorph of VO_2 recovered from high pressure treatment.

The pressure-volume data of *M1*, *M1′*, and *Mx* phases are shown in Fig. 5. The pressure-volume data were fitted to the Birch-Murnaghan EOS

$$P = \frac{3B_0}{2}\left[\left(\frac{V}{V_0}\right)^{\frac{7}{3}} - \left(\frac{V}{V_0}\right)^{\frac{5}{3}}\right]\left\{1 + \frac{3}{4}(B_0' - 4)\left[\left(\frac{V}{V_0}\right)^{-\frac{2}{3}} - 1\right]\right\}$$

where B_0 and B_0' are the isothermal bulk modulus and its pressure derivative, respectively, and V_0 is the unit-cell volume at ambient pressure. B_0' was fixed to 4 for comparison. The best-fit curves were shown as solid lines in Fig. 5a, b, and c. As shown in Table 2, the bulk modulus of the *M1* nanoparticles is higher than that of *M1′* phase. Both of these values for *M1* and *M1′* were higher than those of their bulk counterparts respectively. In addition, the *Mx* phase exhibited a higher bulk modulus than those of the low pressure phases, *M1* and *M1′*, which is less compressible.

To further characterize the pressure-induced phase transitions for VO_2 nanoparticles, high pressure Raman spectroscopy measurements were performed. Fig. 6 shows the Raman spectra of the VO_2 nanoparticles upon compression and decompression. It is known that 9 A_g and 9 B_g Raman active modes are predicted for the *M1* phase [18,39]. In the present study, 11 phonon peaks could be identified at low pressures. phonon peaks at 190, 220, 308, 403, 505, and 630 cm^{-1} are assigned to A_g modes, and those peaks at 265, 362, 450, and 840 cm^{-1} are assigned to B_g modes of the M1 phase [40]. The pressure dependence of the Raman peaks is summarized in Fig. 7. As shown in Figs. 6a and 7, all Raman peaks shown blue shift and broadening with increasing pressure. The blue shift and broadening of the Raman peaks may result from the shrinkage of bond length of VO_2 and the increasing strain with increasing pressure, respectively. The Raman frequencies at ~260 and ~310 cm^{-1} shown clear change on the slope at ~15 GPa, which is related to the *M1*-*M1′* phase transition. Above ~37 GPa, a new peak appeared at ~212 $cm^{-1}$and a sharp increase of the slope for the Raman peak at ~255 cm^{-1} was observed, indicating the phase transition from *M1′* to *Mx*. In addition, the Raman signals of the *M1′* phase became weaker with increasing pressure. Several new peaks were observed at ~450, 480, and 680 cm^{-1} (labeled by stars) above ~42 GPa, which means the *Mx* becomes the dominant phase. Above ~55 GPa, all weak Raman peaks originate from the *Mx* phase. Upon

Table 1
Parameters obtained from the LeBail fit of the XRD patterns of the *Mx* and *Mx′* phases, respectively. R_{wp} and R_p are the weighted profile R-factor and the profile R-factor, respectively.

Phase	Pressure GPa	*a* Å	*b* Å	*c* Å	*β* degree	*V* Å^3	R_{wp} (%)	R_p (%)
Mx	67.9	4.468 (4)	4.693 (3)	4.744 (8)	97.208 (53)	98.699 (183)	0.27	0.16
Mx′	0	4.631 (7)	5.308 (9)	6.394 (7)	101.094 (66)	151.820 (513)	0.35	0.28

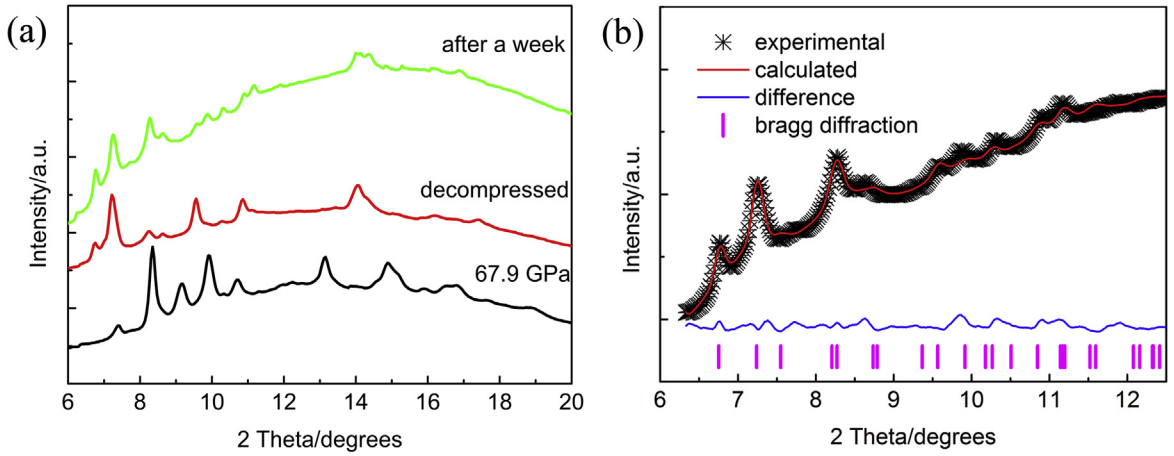


Fig. 4. (a) The XRD patterns of the VO_2 nanoparticles at 67.9 GPa (bottom), decompressed at ambient pressure (middle), and after one week at ambient pressure (top), (b) the XRD pattern of the recovered VO_2 nanoparticles after a week. A monoclinic structure with the same space group as *Mx* is assumed in the refinement.

decompression, all Raman peaks of the *Mx* phase remain down to ~34 GPa. Some new peaks appear at ~31 GPa, indicating a phase transition. With further decreasing pressure, the intensities of these new peaks increased and the peaks of the *Mx* phase disappeared at 23.9 GPa. This indicates that the high pressure *Mx* phase transforms into a new structure completely. The Raman spectrum of the quenched sample is similar to that of the starting *M1* phase, which can be attributed to the similar local structure of the two phases. These Raman results complement the observed phase transitions from the XRD data.

In order to identify the MIT for the VO_2 nanoparticles under high pressure, mid-IR reflectivity R(ω) spectra of the sample were measured. Fig. 8 shows the evolution of the IR reflectivity spectra of the VO_2 nanoparticles under high pressure. With increasing pressure, R(ω) only changed slightly up to 10.8 GPa, and then increased quickly above 13.1 GPa. Above 32.9 GPa, R(ω) increased subtly and almost shown no change when the pressure was beyond 37 GPa. Pressure dependence of the IR reflectivity at two frequencies (inset of Fig. 8a) clearly identifies the electronic change upon compression. The reflectivity increases gradually in the pressure region of 2.7–37 GPa, and becomes nearly independent of the applied pressure above ~37 GPa. At ~32.9 GPa, the *M1′* phase is still the dominant phase according to the XRD and Raman results. These results indicated that a pressure-induced insulator-to-metal transition occurs in the *M1′* phase at ~32.9 GPa. Similar results were observed in VO_2 (*M1*) bulk in which the electrical resistivity shown almost no change in insulating *M1′* and metallic *Mx* phase above ~30 GPa, although the theoretical calculation indicated the band gap does not close in the *M1′* phase up to 40 GPa [22]. It is clear the *Mx* phase was metallic, which was consistent with the previous study [22]. Upon decompression, R(ω) exhibited subtle change in the range of 29.4–58.1 GPa. With further decreasing pressure, R(ω) decreased significantly below 19.3 GPa. These reflectivity results are directly associated with the phase transitions from the high pressure *Mx* phase to the low pressure phases. The structural transitions thus appear to be responsible for the MIT in VO_2 nanoparticles upon decompression.

The *M1* phase of VO_2 consists of VO_6 octahedra with alternating V-V distances of 2.654 and 3.125 Å zigzag chains along the *a* axis (originates from the *c* axis in the metallic *R* phase), in contrast to the unique V-V distances along the *c* axis in the *R* phase. The MIT of the *M1*-*R* phase transition has been explained by the paired V-V formation, which results in splitting the half-filled d_η orbital in the *R* phase into fully filled orbital d_η and empty orbital π^* in the *M1* phase. Previous studies have indicated that the V-V distances strongly influence the phase transitions and electronic properties [15,41]. It is worth noting that ω_{V1} (~190 cm^{-1}) and ω_{V2} (~220 cm^{-1}) Raman peaks were assigned to the V-ions motion in the dimerized chains, the ω_o peak at ~620 cm^{-1} was ascribed to a V-O mode that mainly involves the oxygen ions connecting with the different V chains along the *c*-axis, while the lowest Raman mode at ~180 cm^{-1} is related to the octahedral rotation mode [18,19]. Thus, the slight slope change of these modes at the first phase transition pressure (~15 GPa) suggested that both the V-V dimerized chains and VO_6 octahedra were stable during the *M1*-*M1′* phase transition. However, the sharp slope change of ω_{V2} peak above ~37 GPa shown that the significant change and rearrangement of V-V bonds occurred in the phase transition from *M1′* to *Mx*. The vanishing of ω_{V1} and ω_{V2} peaks at higher pressure is likely related to destruction of V-V dimers which resulted in the metallization in the *Mx* phase. Upon decompression, the *Mx* phase transformed into another structure with the reappearance of these ω_{V1} and ω_{V2} peaks. This indicates that the V-V dimers formed in the quenched phase, which may contribute to the MIT upon decompression.

The pressure dependence of reflectivity in *M1′* phase (the inset of Fig. 8a) suggested that the carrier concentration increases upon compression, indicating that the *M1′* phase is likely semimetallic [42]. According to previous studies [15,41], there exists a critical V-V distance (2.94 Å) for VO_2. When the V-V distance is less than the critical distance, the coupling interaction between *3d* electrons

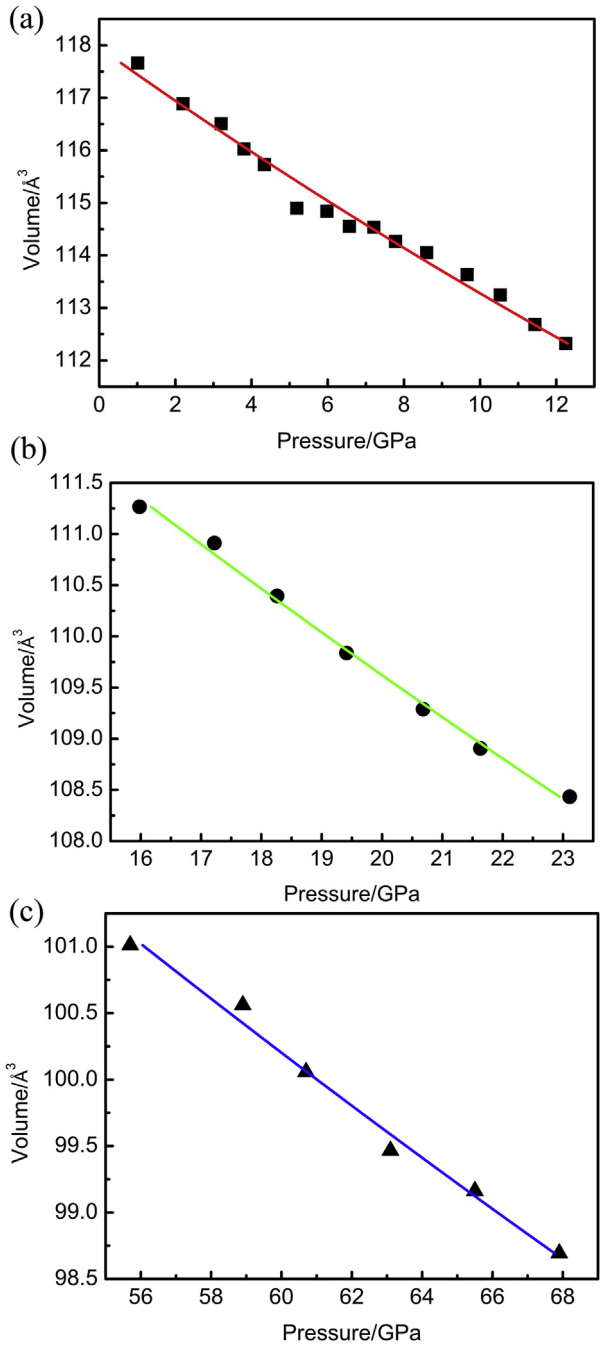


Fig. 5. Pressure-volume diagram of the *M1* (a), *M1′* (b), and *Mx* (c) phases of VO_2 nanoparticles.

Table 2
Comparison of the EOS parameters with different phases in VO_2. B_0' was fixed to 4 for comparison.

Phase	V_0 (Å^3)	B_0 (GPa)	Reference
M1	117.96 (13)	228 (9)	This study
M1	117.98 (4)	142 (1)	Ref [21]
M1	118.32 (4)	213 (2)	Ref [22]
M1′	119.84 (37)	188 (8)	This study
M1′	120.20 (30)	167 (4)	Ref [22]
Mx	117.45 (56)	275 (25)	This study

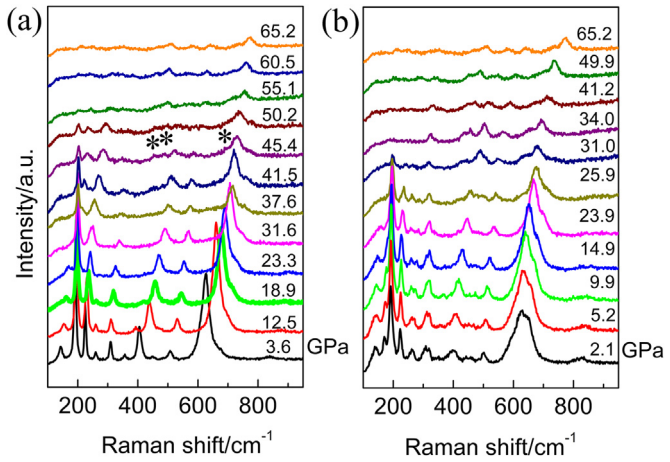


Fig. 6. High pressure Raman spectra of VO_2 nanoparticles: (a) compression, (b) decompression.

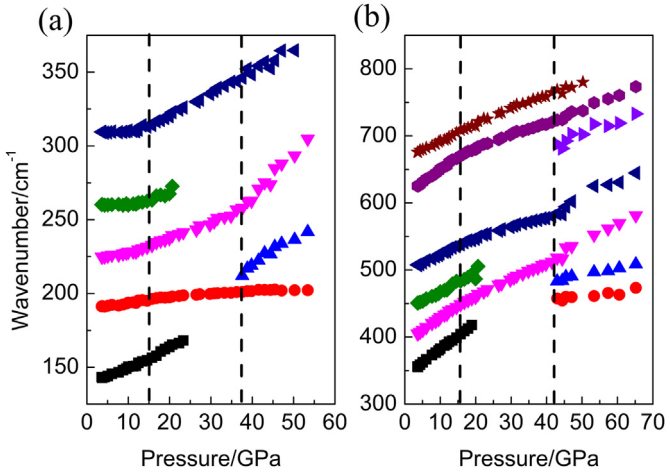


Fig. 7. Pressure dependencies of the observed Raman modes upon compression. (a) Phonon modes between 100 and 350 cm^{-1}, and (b) phonon modes between 350 and 800 cm^{-1}.

leads to the itinerant electronic behavior. In the starting *M1* phase, the longer V-V distance (3.125 Å) is sufficiently larger than the critical distance. Thus the *d*-orbital electrons are localized within the shorter V-V dimers, leading to the insulating behavior. The lattice compression with increasing pressure was observed in XRD results. Therefore, it is likely that the V-V distance becomes comparable with or even less than the critical value in the *M1′* phase without structural phase transition at pressures above ~32.9 GPa, which may have caused the delocalization of V *3d* electrons. According to the XRD, Raman and IR reflectivity results, the pressure-induced metallization which happened within the *M1′* phase was caused by the strong electron correlations (Mott effect). In contrast, the MIT upon decompression was related to the structural phase transitions. Compared with the temperature driven MIT, the pressure driven MIT could decouple the structural and electronic phase transition in VO_2.

It is well known that high pressure phase transition behaviors can be tuned by the grain size of nanomaterials. Enhanced transition pressure with decreasing particle size has been demonstrated in many nanomaterials, such as ZnS [43], SnO_2 [44], and ZnO [45], which has been interpreted as being caused by the high surface energy of nanoparticles. However, reduced transition pressure with

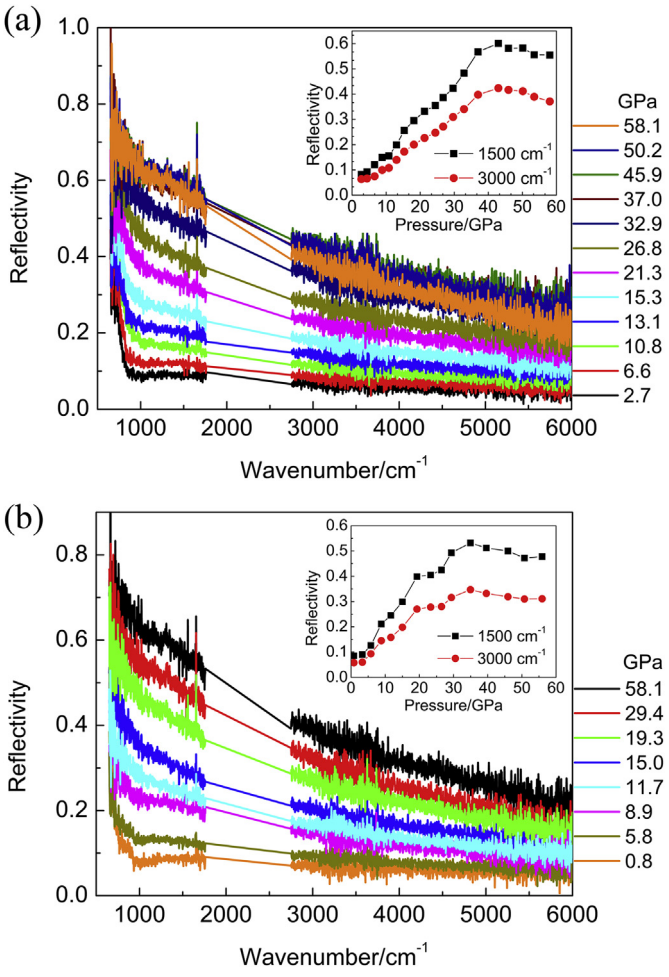


Fig. 8. IR reflectivity spectra of VO_2 nanoparticles upon compression (a) and decompression (b). The insets are the plots of reflectivity as a function of pressure for two different wave numbers (1500 and 3000 cm^{-1}). A portion of the spectrum in the range of 1750–2750 cm^{-1} is not shown due to the strong absorption by diamond.

decreased particle size was observed in some other nanomaterials such as CeO_2 [46] and Fe_2O_3 [47], which has been explained in terms of a large volume collapse during the phase transition. For VO_2 nanoparticles, the transition pressure from *M1* to *M1′* was above 14.9 GPa, which is higher than those of their bulk counterparts (12–13 GPa) [21,22]. In addition, the bulk moduli for *M1* (228 GPa) and *M1′* (188 GPa) nanoparticles are higher than those of the corresponding bulk materials, 142 and 213 GPa for *M1* [21,22], and 167 GPa for *M1′* [22], respectively. It is reasonable that the surface energy of VO_2 nanoparticles is higher than that of the macrocrystals, thus the enhanced transition pressure and bulk modulus can be attributed to their high surface energy caused by nanosize effects. Moreover, the nanosize of VO_2 particles is likely less than the characteristic domain size of VO_2. The nanosized VO_2 can exclude or significantly reduce the interference from grain boundary connectivity and domain dynamics in macrocrystals. Therefore, these electronic properties and structural phase transition behaviors in nanosized VO_2 are likely more close to the inherent characters of VO_2.

4. Conclusions

In summary, pressure-induced phase transitions and insulator-metal transitions in VO_2 nanoparticles were studied by synchrotron x-ray diffraction, Raman spectroscopy, and infrared reflectivity spectra. The isostructural phase transition of *M1-M1′* was observed above ~14.9 GPa. Upon further compression, the structural phase transition *M1′-Mx* occurred above ~32 GPa. Upon decompression, the *Mx* phase transformed into mixed phases and further converts into a new monoclinic phase (*Mx′*) after a week. The reflectivity of VO_2 increased gradually with increasing pressure, and then remained roughly constant above ~37 GPa. These results indicated that the pressure-induced metallization occurred in the *M1′* phase and it could be attributed to the electron-electron correlations. The MIT under decompression is dominated by the structural phase transition. Compared to bulk materials, VO_2 nanoparticles shown larger bulk moduli and increased transition pressure due to their nanosize effects. Both the electron-correlation-driven Mott transition and the structure-driven MIT could be achieved in VO_2 by applying pressure. Induced-pressure phase transition provided an effective method to study the MIT in strongly correlated materials, and a potential way to modify electronic properties of materials.

Acknowledgments

This work was financially supported by the NSFC (11374120 and 51320105007), National Basic Research Program of China (2011CB808200), Program for Changjiang Scholars and Innovative Research Team in University (No. IRT1132), the visiting scholar project funded by China Scholarship Council, and the Cheung Kong Scholars Programme of China. This research was performed at HPCAT (sector 16), Advanced Photon Source (APS), Argonne National Laboratory. HPCAT operations are supported by DOE-NNSA under Award No. DE-NA0001974 and DOE-BES under Award No. DE-FG02-99ER45775, with partial instrumentation funding by NSF. The APS is a U. S. Department of Energy (DOE) Office of Science User Facility operated for the DOE Office of Science by ANL under Contract No. DE-AC02-06CH11357. We thank Stanislav V. Sinogeikin and Curtis Kenney-Benson for technical assistance.

References

[1] M. Imada, A. Fujimori, Y. Tokura, Metal-insulator transitions, Rev. Mod. Phys. 70 (1998) 1039–1263.
[2] F.J. Morin, Oxides which show a metal-to-insulator transition at the Neel temperature, Phys. Rev. Lett. 3 (1959) 34–36.
[3] J.D. Budai, J. Hong, M.E. Manley, E.D. Specht, C.W. Li, J.Z. Tischler, D.L. Abernathy, A.H. Said, B.M. Leu, L.A. Boatner, R.J. McQueeney, O. Delaire, Metallization of vanadium dioxide driven by large phonon entropy, Nature 515 (2014) 535–539.
[4] H.-T. Kim, Y.W. Lee, B.-J. Kim, B.-G. Chae, S.J. Yun, K.-Y. Kang, K.-J. Han, K.-J. Yee, Y.-S. Lim, Monoclinic and correlated metal phase in VO_2 as evidence of the Mott transition: coherent phonon analysis, Phys. Rev. Lett. 97 (2006) 266401.
[5] S.A. Corr, D.P. Shoemaker, B.C. Melot, R. Seshadri, Real-space investigation of structural changes at the metal-insulator transition in VO_2, Phys. Rev. Lett. 105 (2010) 56404.
[6] W.-P. Hsieh, M. Trigo, D.A. Reis, G. Andrea Artioli, L. Malavasi, W.L. Mao, Evidence for photo-induced monoclinic metallic VO_2 under high pressure, Appl. Phys. Lett. 104 (2014) 21917.
[7] C.N. Berglund, H.J. Guggenheim, Electronic properties of VO_2 near the semiconductor-metal transition, Phys. Rev. 185 (1969) 1022–1033.
[8] J. Laverock, S. Kittiwatanakul, A.A. Zakharov, Y.R. Niu, B. Chen, S.A. Wolf, J.W. Lu, K.E. Smith, Direct observation of decoupled structural and electronic transitions and an ambient pressure monocliniclike metallic phase of VO_2, Phys. Rev. Lett. 113 (2014) 216402.
[9] M. Yang, Y. Yang, Bin Hong, L. Wang, K. Hu, Y. Dong, H. Xu, H. Huang, J. Zhao, H. Chen, L. Song, H. Ju, J. Zhu, J. Bao, X. Li, Y. Gu, T. Yang, X. Gao, Z. Luo, C. Gao, Suppression of structural phase transition in VO_2 by epitaxial strain in vicinity of metal-insulator transition, Sci. Rep. 6 (2016) 23119.
[10] G. Villeneuve, P. Hagenmuller, Metal-insulator transitions in pure and doped VO_2, Localization and metal-insulator transitions, Springer, US, 1985, pp. 39–52.
[11] T.M. Rice, H. Launois, J.P. Pouget, Comment on "VO_2: Peierls or Mott-Hubbard? A view from band theory", Phys. Rev. Lett. 73 (1994) 3042.
[12] M.M. Qazilbash, M. Brehm, B.-G. Chae, P.-C. Ho, G.O. Andreev, B.-J. Kim,

S.J. Yun, A.V. Balatsky, M.B. Maple, F. Keilmann, H.-T. Kim, D.N. Basov, Mott transition in VO_2 revealed by infrared spectroscopy and nano-imaging, Science 318 (2007) 1750–1753.
[13] J. Cao, W. Fan, K. Chen, N. Tamura, M. Kunz, V. Eyert, J. Wu, Constant threshold resistivity in the metal-insulator transition of VO_2, Phys. Rev. B 82 (2010) 241101.
[14] J.B. Goodenough, The two components of the crystallographic transition in VO_2, J. Solid State Chem. 3 (1971) 490–500.
[15] R.M. Wentzcovitch, W.W. Schulz, P.B. Allen, VO_2: Peierls or Mott-Hubbard? A view from band theory, Phys. Rev. Lett. 72 (1994) 3389–3392.
[16] M.W. Haverkort, Z. Hu, A. Tanaka, W. Reichelt, S.V. Streltsov, M.A. Korotin, V.I. Anisimov, H.H. Hsieh, H.-J. Lin, C.T. Chen, D.I. Khomskii, L.H. Tjeng, Orbital-assisted metal-insulator transition in VO_2, Phys. Rev. Lett. 95 (2005) 196404.
[17] T.C. Koethe, Z. Hu, M.W. Haverkort, C. Schüßler-Langeheine, F. Venturini, N.B. Brookes, O. Tjernberg, W. Reichelt, H.H. Hsieh, H.-J. Lin, C.T. Chen, L.H. Tjeng, Transfer of spectral weight and symmetry across the metal-insulator transition in VO_2, Phys. Rev. Lett. 97 (2006) 116402.
[18] E. Arcangeletti, L. Baldassarre, D. Di Castro, S. Lupi, L. Malavasi, C. Marini, A. Perucchi, P. Postorino, Evidence of a pressure-induced metallization process in monoclinic VO_2, Phys. Rev. Lett. 98 (2007) 196406.
[19] C. Marini, E. Arcangeletti, D. Di Castro, L. Baldassare, A. Perucchi, S. Lupi, L. Malavasi, L. Boeri, E. Pomjakushina, K. Conder, P. Postorino, Optical properties of $V_{1-x}Cr_xO_2$ compounds under high pressure, Phys. Rev. B 77 (2008) 235111.
[20] A. Perucchi, L. Baldassarre, P. Postorino, S. Lupi, Optical properties across the insulator to metal transitions in vanadium oxide compounds, J. Phys. Condens. Matter 21 (2009) 323202.
[21] M. Mitrano, B. Maroni, C. Marini, M. Hanfland, B. Joseph, P. Postorino, L. Malavasi, Anisotropic compression in the high-pressure regime of pure and chromium-doped vanadium dioxide, Phys. Rev. B 85 (2012) 184108.
[22] L. Bai, Q. Li, S.A. Corr, Y. Meng, C. Park, S.V. Sinogeikin, C. Ko, J. Wu, G. Shen, Pressure-induced phase transitions and metallization in VO_2, Phys. Rev. B 91 (2015) 104110.
[23] X. Zhang, J. Zhang, F. Ke, G. Li, Y. Ma, X. Liu, C. Liu, Y. Han, Y. Ma, C. Gao, Anomalous semiconducting behavior on VO_2 under high pressure, RSC Adv. 5 (2015) 54843–54847.
[24] J. Wei, Z. Wang, W. Chen, D.H. Cobden, New aspects of the metal–insulator transition in single-domain vanadium dioxide nanobeams, Nat. Nanotechnol. 4 (2009) 420–424.
[25] T. Favaloro, J. Suh, B. Vermeersch, K. Liu, Y. Gu, L.-Q. Chen, K.X. Wang, J. Wu, A. Shakouri, Direct observation of nanoscale Peltier and Joule effects at metal–insulator domain walls in vanadium dioxide nanobeams, Nano Lett. 14 (2014) 2394–2400.
[26] J. Wu, Q. Gu, B.S. Guiton, N.P. de Leon, L. Ouyang, H. Park, Strain-Induced Self Organization of metal–insulator domains in single-crystalline VO_2 nanobeams, Nano Lett. 6 (2006) 2313–2317.
[27] S. Zhang, J.Y. Chou, L.J. Lauhon, Direct correlation of structural domain formation with the metal insulator transition in a VO_2 nanobeam, Nano Lett. 9 (2009) 4527–4532.
[28] L. Whittaker, C.J. Patridge, S. Banerjee, Microscopic and nanoscale perspective of the metal–insulator phase transitions of VO_2: some new twists to an old tale, J. Phys. Chem. Lett. 2 (2011) 745–758.
[29] H. Asayesh-Ardakani, A. Nie, P.M. Marley, Y. Zhu, P.J. Phillips, S. Singh, F. Mashayek, G. Sambandamurthy, K. Low, R.F. Klie, S. Banerjee, G.M. Odegard, R. Shahbazian-Yassar, Atomic origins of monoclinic-tetragonal (rutile) phase transition in doped VO_2 nanowires, Nano Lett. 15 (2015) 7179–7188.
[30] P. Zukowski, T.N. Koltunowicz, V. Bondariev, A.K. Fedotov, J.A. Fedotova, Determining the percolation threshold for $(FeCoZr)_x(CaF_2)_{(100-x)}$ nanocomposites produced by pure argon ion-beam sputtering, J. Alloy. Compd. 683 (2016) 62–66.
[31] M. Ghiyasiyan-Arani, M. Masjedi-Arani, M. Salavati-Niasari, Size controllable synthesis of cobalt vanadate nanostructures with enhanced photocatalytic activity for the degradation of organic dyes, J. Mol. Catal. A Chem. 425 (2016) 31–42.
[32] F. Mazloom, M. Masjedi-Arani, M. Salavati-Niasari, Controllable synthesis, characterization and photocatalytic studies on cadmium vanadate nanostructures, J. Mol. Liq. 220 (2016) 566–572.
[33] R. Lopez, T.E. Haynes, L.A. Boatner, L.C. Feldman, R.F. Haglund, Size effects in the structural phase transition of VO_2 nanoparticles, Phys. Rev. B 65 (2002) 224113.
[34] R. Lopez, L.C. Feldman, R.F. Haglund, Size-dependent optical properties of VO_2 nanoparticle arrays, Phys. Rev. Lett. 93 (2004) 177403.
[35] J.I. Sohn, H.J. Joo, D. Ahn, H.H. Lee, A.E. Porter, K. Kim, D.J. Kang, M.E. Welland, Surface-stress-induced Mott transition and nature of associated spatial phase transition in single crystalline VO_2 nanowires, Nano Lett. 9 (2009) 3392–3397.
[36] S. Sudeshna, Q.J. Li, B.Y. Cheng, Y.W. Huang, C.Y. Pei, Q.L. Wang, Y.Z. Ma, L. Wang, Phase coexistence and pressure-temperature phase evolution of VO_2 (A) nanorods near the semiconductor-semiconductor transition, Phys. Rev. B 95 (2017) 045135.
[37] H. Zhang, Q. Li, P. Shen, Q. Dong, B. Liu, R. Liu, T. Cui, B. Liu, The structural phase transition process of free-standing monoclinic vanadium dioxide micron-sized rods: temperature-dependent Raman study, RSC Adv. 5 (2015) 83139–83143.
[38] B.H. Toby, EXPGUI, a graphical user interface for GSAS, J. Appl. Crystallogr. 34 (2001) 210–213.
[39] R. Srivastava, L.L. Chase, Raman spectrum of semiconducting and metallic VO_2, Phys. Rev. Lett. 27 (1971) 727–730.
[40] H.T. Kim, B.G. Chae, D.H. Youn, G. Kim, K.Y. Kang, S.J. Lee, K. Kim, Y.S. Lim, Appl. Phys. Lett. 86 (2005) 242101.
[41] T. Yao, X. Zhang, Z. Sun, S. Liu, Y. Huang, Y. Xie, C. Wu, X. Yuan, W. Zhang, Z. Wu, G. Pan, F. Hu, L. Wu, Q. Liu, S. Wei, Understanding the nature of the kinetic process in a VO_2 metal-insulator transition, Phys. Rev. Lett. 105 (2010) 226405.
[42] Y. Mita, D. Izaki, M. Kobayashi, S. Endo, Pressure-induced metallization of MnO, Phys. Rev. B 71 (2005) 100101.
[43] Z. Wang, L.L. Daemen, Y. Zhao, C.S. Zha, R.T. Downs, X. Wang, Z.L. Wang, R.J. Hemley, Morphology-tuned wurtzite-type ZnS nanobelts, Nat. Mater 4 (2005) 922–927.
[44] Y. He, J.F. Liu, W. Chen, Y. Wang, H. Wang, Y.W. Zeng, G.Q. Zhang, L.N. Wang, J. Liu, T.D. Hu, H. Hahn, H. Gleiter, J.Z. Jiang, High-pressure behavior of SnO_2 nanocrystals, Phys. Rev. B 72 (2005) 212102.
[45] L. Wang, H. Liu, J. Qian, W. Yang, Y. Zhao, Structural stability and compressibility study for ZnO nanobelts under high pressure, J. Phys. Chem. C 116 (2012) 2074–2079.
[46] Z. Wang, S.K. Saxena, V. Pischedda, H.P. Liermann, C.S. Zha, *In situ* x-ray diffraction study of the pressure-induced phase transformation in nanocrystalline CeO_2, Phys. Rev. B 64 (2001) 12102.
[47] J.Z. Jiang, J.S. Olsen, L. Gerward, S. Morup, Enhanced bulk modulus and reduced transition pressure in γ-Fe_2O_3 nanocrystals, Europhys. Lett. 44 (1998) 620.